# Dielectric Performance of Composites of $BaTiO_3$ and Polymers for Capacitor Applications under Microwave Frequency

**S. Bahar Basturk[1,2]*, Claire E. J. Dancer[2], Tony McNally[2]**

[1]Department of Metallurgy and Materials Engineering, Manisa Celal Bayar University, 45040,Turkey

[2]Internationational Institute for Nanocomposite Manufacturing (IINM), WMG, University of Warwick, CV4 7AL, UK.

Corresponding Author: Bahar Basturk, e-mail: bahar.basturk@cbu.edu.tr

## Abstract

Composites of nano-sized barium titanate ($BaTiO_3$) with volume fractions up to 0.5 and poly(butylene terephthalate) (PBT) or low density polyethylene (LLDPE) were made via extrusion. Scanning electron microscopy (SEM) demonstrated that $BaTiO_3$ is well-dispersed in the polymer matrices. Unexpectedly, the crystalline content (DSC) and thermal stability (TGA) of both polymers decreased with increasing $BaTiO_3$ loading. Dielectric properties of the composites were measured using a vector network analyser (VNA). Both dielectric permittivity and tangent loss increased with increasing $BaTiO_3$ content. At 2.45 GHz, the dielectric permittivity for 48 vol% $BaTiO_3$-filled LLDPE and 43 vol% $BaTiO_3$-filled PBT was 25 and 21.2, respectively. There was a good fit between the Lichtenecker model and experimental data obtained up to a certain value, with the permittivity variations being dependent on volume fraction. The improved dielectric performance achieved on inclusion

of $BaTiO_3$ confirms both composite systems as potential candidates for microwave frequency capacitor applications.

## 1. Introduction

The widespread utilization of electronic equipment in many different industries including communications, automotive, power/energy applications, military, robotics, medical and aerospace requires printed circuit boards (PCBs). Fundamentally PCBs, which are the main components of electronic products, consist of a substrate supporting passive electronic devices (e.g. capacitors, transistors, diodes and resistors). A low dielectric permittivity is required for the substrate component to reduce the signal propagation delay while passive elements such as capacitors generally exhibit a higher dielectric permittivity, needed to store energy. In conventional passive electronic devices the PCB constituents are made of paraelectric or ferroelectric ceramics because of their high dielectric character. Although the capacitors produced from ceramics are excellent dielectric materials, their brittle structure give rise to many manufacturing problems due to high processing temperatures that are not usually compatible with circuit integration technologies. Conversely, polymers with low dielectric constants can have ductile properties, which facilitates the fabrication of complex geometries at relatively cheaper cost [1-5]. Composite materials composed of a flexible polymer matrix and high dielectric ceramic fillers are promising and effective alternatives for new generation PCBs instead of conventional counterparts [6]. The production of polymeric composites based on ceramics such as lead magnesium niobate–lead titanate (PMN–PT) [7-9], calcium barium zirconate titanate (BCZT) [10], lead titanate based (PSTM) [11], lead-magnezium-niobate (PMN) [12] and lead zirconium titanate (PZT) [13-14] have

been reported in the literature. However, in both academia and industry the application of lead-based capacitors have been limited due to their known hazardous and toxic effects. Barium titanate ($BaTiO_3$), a member of the perovskite group of materials like some lead derived ceramics, exhibit excellent dielectric, piezoelectric, and electro-optic properties because of its crystal structure (i.e. a general stoichiometry of $ABO_3$) [2]. Previous studies on both pristine $BaTiO_3$ powder and $BaTiO_3$-based hybrid structures have been conducted in order to determine their dielectric performance. Composites based on $BaTiO_3$ and different types of polymers such as PVDF [15], PVDF-HFP [16], PMMA [17], polyimide [18], polystyrene [19], epoxy [20], PDMS [21], and cellulosic polymers [22] have been prepared. So called "0-3 connected-type composites" have also been reported in the literature, which consist of randomly dispersed ceramic particles in a polymer matrix. Many of the studies in the literature consist of 0-3 type composites that were fabricated using different techniques. Although the dielectric permittivities of thermoplastic polymers range between only 2 and 5, they are very attractive candidates for 0-3 composites due to being easy to process and their widespread availability and relatively low cost [13,23]. The dielectric properties of composites depend on parameters such as permittivity and electrical conductivity of both phases as well as size, volume fraction, and the extent of ceramic filler dispersion and distribution in the polymer matrix. Additionally, the dielectric characteristics of such composites vary as a function of frequency and temperature [4]. Much of the published literature reports the dielectric properties of $BaTiO_3$-based composites analyzed below 10 MHz due to the complexity of specimen production for high frequency measurements. However, electronic devices such as mobile phones, laptops, PCs and tablets are exposed to higher frequencies, typically 2.45 GHz.

In this study we report the dielectric response of composites consisting of either a polar polymer, poly(butylene terephthalate) (PBT)/$BaTiO_3$, or a non-polar polymer, linear low density polyethylene (LLDPE)/$BaTiO_3$, in the 2.45 to 5 GHz wireless communication frequency range. All composite materials were prepared using extrusion, a continuous and scalable process, with $BaTiO_3$ volume loadings up to 50 vol.%. The thermal, crystalline and morphology of the composites produced were characterised using a range of thermal, spectroscopic, and microscopic techniques and correlated with measurements of the dielectric response of the composites in the 2.45-5GHz frequency range.

## 2. Experimental Section

### 2.1. Materials

Granulated polybutylene terephthalate (PBT) grade Pocan B 1700000000 was purchased from Lanxess™, Germany and linear low density polyethylene (LLDPE) was provided by Terplast™, Italy. Barium titanate ($BaTiO_3$) ceramic nanopowder (HPB 4000) with an average particle size of 400 nm was supplied by TPL™, USA.

### 2.2. Preparation of Composites

Figure 1 shows a schematic representation of the preparation steps used in the production of the composite materials. Firstly, PBT or LLDPE granules were ground to powder form via cryo-milling with liquid $N_2$ in a Freezer Mill (SPEX™) machine to provide more intimate mixing of the blend constituents. Then the required amount of nanofiller (10%, 20%, 30%, 40% and 50% vol. $BaTiO_3$) and matrix (PBT or LLDPE) were dry blended by shaking. The resultant mixture was dried in an vacuum oven at 100°C overnight to remove moisture, as

the PBT is hydroscopic, using the drying conditions recommended by the manufacturer. Prior to extrusion, the dried hybrid blend was mechanically mixed to incorporate the filler with the polymer. The composite samples were prepared using a Thermo Scientific™ co-rotating 24 mm twin-screw extruder operating a temperature profile over 10 zones. The temperature values varied from the feed to die end along the barrel and were set between 215°C to 250°C and 135°C to 145°C for PBT/ $BaTiO_3$ and LLDPE/ $BaTiO_3$ composites, respectively. Throughout this process, the screw speed was kept constant at 40 rpm while the composites were prepared. The composite forumalations of PBT or LLDPE with various $BaTiO_3$ volume ratios are given in Table 1.

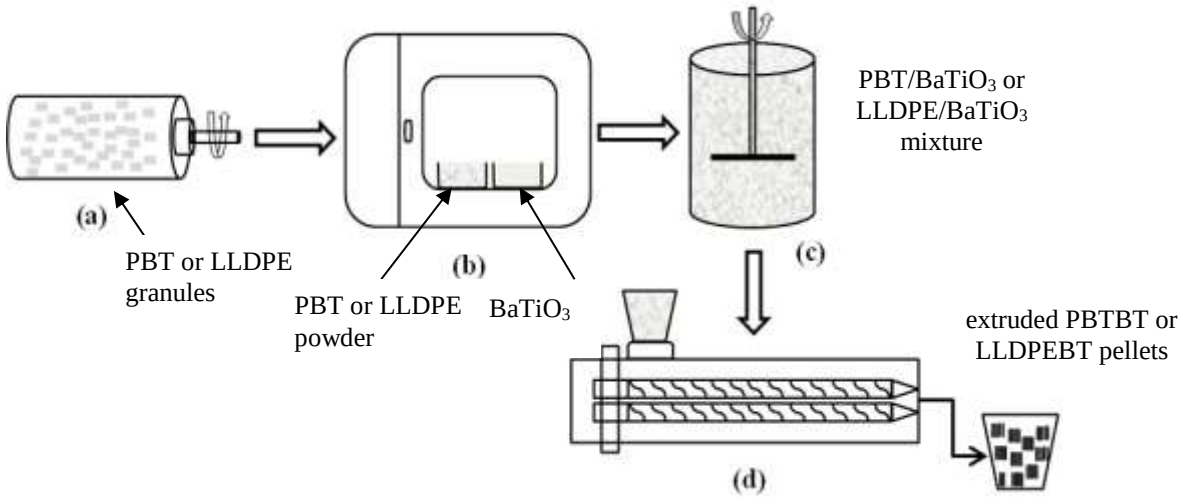


**Figure 1.** Schematic illustration of the preperation steps for $BaTiO_3$ based composites: a) cryo-milling of granulated PBT or LLDPE polymers, b) drying of $BaTiO_3$, PBT and LLDPE, c) mechanical mixing of dried powders and d) extrusion of PBTBT and LLDPEBT composites.

**Table 1.** Formulations of composites prepared.

| Sample Code | Theoretical $BaTiO_3$ content (vol.%) | Theoretical PBT content (vol.%) | Theoretical LLDPE content (vol.%) |
|---|---|---|---|
| PBT | - | 100 | - |
| PBTBT10 | 10 | 90 | - |
| PBTBT20 | 20 | 80 | - |
| PBTBT30 | 30 | 70 | - |
| PBTBT40 | 40 | 60 | - |
| PBTBT50 | 50 | 50 | - |
| LLPDE | - | - | 100 |
| LLDPEBT10 | 10 | - | 90 |
| LLDPEBT20 | 20 | - | 80 |
| LLDPEBT30 | 30 | - | 70 |
| LLDPEBT40 | 40 | - | 60 |
| LLDPEBT50 | 50 | - | 50 |

2.3. Characterization

The thermal properties of all materials were studied using differential scanning calorimetry (DSC) using a Mettler Toledo DSC1 calorimeter under nitrogen flow. The ~5-10 mg samples were firstly heated to 250°C at 10 K/min. and kept at this temperature for 5 minutes to eliminate thermal history. Then, the samples were cooled at 10 K/min. to ambient temperature, followed by a second heating cycle up to 250°C, again at a rate of 10 K/min. The thermal stability of all materials was investigated using thermogravimetric analysis

(TGA), performed using a Mettler Toledo Simultaneous Thermal Analysis instrument. An alumina crucible was used as the reference material and the experiments were conducted at a heating rate of 10 K/min from 25°C to 800°C in an air atmosphere. Infrared spectra of the composites were recorded using a Bruker Tensor™-27 Fourier transform infrared (FTIR) spectrometer. The attenuated total reflectance (ATR) technique was employed with a scan number of 32 used over the wavelength range 4000-500 $cm^{-1}$. The X-Ray diffraction (XRD) patterns of all materials were collected using a Panalytical Empyrean™ system with Co ($K_\alpha$=1.789$\AA$) radiation in a wide range of $2\theta$ ($20° \leq 2\theta \leq 80°$). The approximate content of $BaTiO_3$ crystal phases were determined by carrying out a whole spectrum Rietveld refinement using the High Score Plus software program.

Representative extruded $BaTiO_3$/PBT and $BaTiO_3$/LLDPE composite samples were examined using a Carl Zeiss™ Sigma Field Emission Gun–Scanning Electron Microscope (FEG-SEM) to image the filler morphology and examine the degree of $BaTiO_3$ dispersion throughout the polymer matrix. All samples were sputter coated with Au prior to being analysed by back scattering and secondary electron imaging modes under an accelerating voltage between 2-10 kV. Dielectric measurements at the relatively high frequency range (2.45-5 GHz) were performed using a two-port Vector Network Analyzer (VNA, Keysight Agilent N1500A) and a co-axial probe method. The cylindrical PBTBT and LLDPEBT dielectric samples with 7 mm diameter were manufactured with a bespoke hot pressing technique at 245°C and 135°C under 10 bar pressure, respectively, and cut to exact dimensions as determined from the estimated filler content (see Fig-S1). The dielectric

permitivitty (or real part permitivitty-$\varepsilon'$) and loss tangent ($tan\delta$) parameters were obtained from the S-parameters using the Nicolson-Ross-Weir approach [24].

## 3. Results and Discussion

### 3.1. Morphological Characterization

Figure 2(a)-(f) shows the FEG-SEM images of as-received nano-barium titanate powder and cross-sections of PBTBT-based composites with various $BaTiO_3$ concentrations. The composites produced during extrusion form a filament which is then cooled in a water bath and any orientation is frozen in to the composite structure. Thus, it is highly probable that some degree of alignment of the polymer and $BaTiO_3$ particles result. From the micrographs it can be clearly observed that melt mixing resulted in well-dispersed ceramic particles in the PBT matrix, independent of filler concentration. It is also seen from the same images that, as the amount of $BaTiO_3$ added was increased, more particles can be seen on the surface, as expected. Although some filler agglomerates were apparent in the composites (particularly for the PBTBT50 sample), uniform distribution of the $BaTiO_3$ was generally achieved. The presence of some porosity of various dimensions, indicates relatively poor interaction between the matrix and the ceramic filler, by way of example see Figure 2 (b) and (c). Furthermore, there are small voids/cavities in the structure that are attributed to the $BaTiO_3$ particles being pulled out of the PBT matrix during fracturing. This type of morphology can be clearly seen from the inset of Figure 2 (e) and provides evidence of the limited bonding between the composite components.

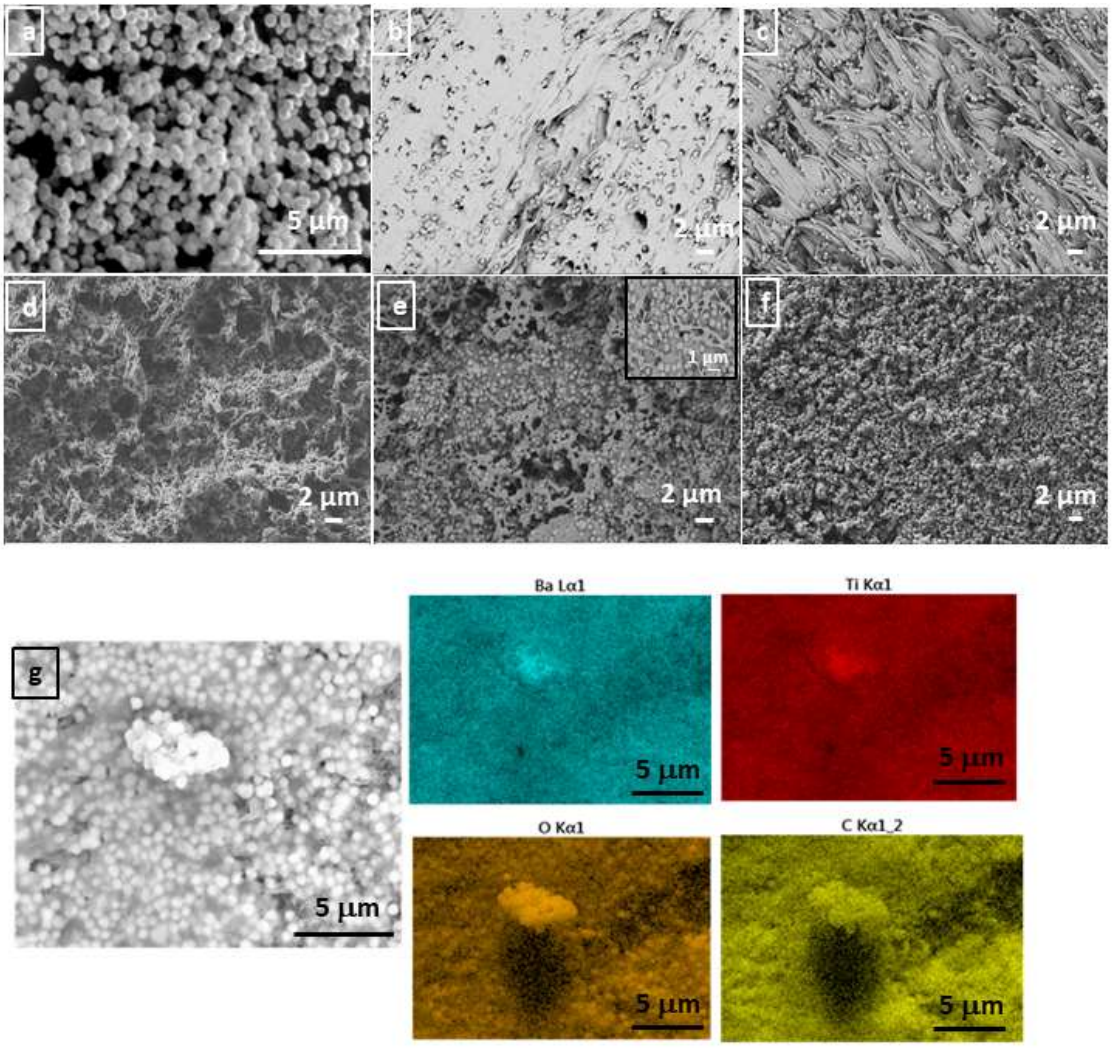


**Figure 2.** SEM micrographs of (a) pristine $BaTiO_3$ powder, (b) PBTBT10 (c) PBTBT20, (d) PBTBT30, (e) PBTBT40, (f) PBTBT50 and (g) EDS elemental mapping of PBTBT40.

Elemantal mapping image (see Figure 2-g) shows the composition of Ba, Ti, O and C elements in the PBTBT40 composite to accurately reveal the microstructural homogenity of the sample. Figures 3 (a-e) are typical SEM images of specimens taken from the LLDPEBT composites. The $BaTiO_3$ particles are positioned interstitially within the fibrous LLDPE

matrix and are generally uniformly dispersed and distributed. However, with further addition of $BaTiO_3$, crowding of the ceramic phase results where there is continuous contact between particles. Minor clustering and/or agglomeration occurs and are observed in the microstructures of the composite samples, see Figure 3 (e). Additionally, there appears to be a degree of adhesion between the LLDPE fibrils and the $BaTiO_3$, particularly in Figure 3 (d) and (e).

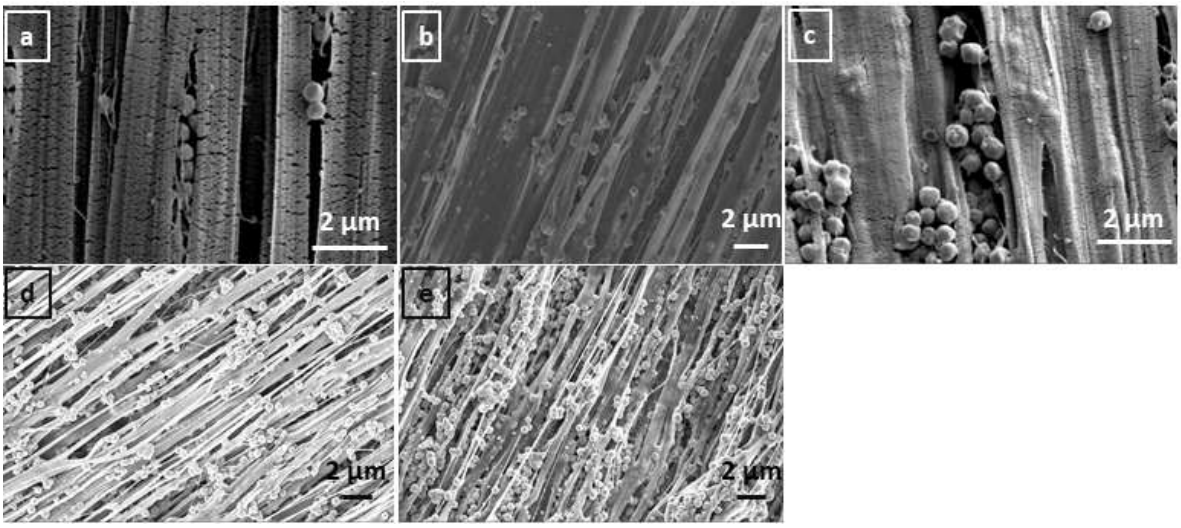


**Figure 3.** SEM micrographs of composites of (a) LLDPEBT10, (b) LLDPEBT20, (c) LLDPEBT30, (d) LLDPEBT40 and (e) LLDPEBT50

3.2. XRD Analysis

The X-ray profiles of the raw materials and their composites are shown in Figure 4. The diffraction peaks associated with the corresponding crystal planes of $BaTiO_3$ are observed in Figure 4(a). It is well known that the high dielectric permittivity of perovskite ceramics derives from their tetragonal crystal structures [25]. Therefore, the crystal types in the

ceramic powder is of great importance and scientific interest. In particular, the presence of the (200) and/or (002) plane in the $BaTiO_3$ structure is the major indicator for the presence of cubic and tetragonal phases. The splitting of the peak(s) at about 53°(2θ), magnified and shown in Figure 4 (b) confirms the presence of both phases. Using the same figure, plotted by considering Rietveld analysis, the as-received $BaTiO_3$ used in this study is composed of approaximately 70% tetragonal and 30% cubic crystal phase (see Figure-S2). $BaCO_3$ and $BaCl_2$ were also detected as minor phases present in the same ceramic material. Figure 4 (c) and (d) show the changes in the crystalline features of the composites of LLDPE and PBT and $BaTiO_3$ as a function of $BaTiO_3$ content. The characteristic diffraction peaks of $BaTiO_3$ are also evident in XRD profiles of composite samples. From Figure 4 (c) it was found that the introduction of ceramic filler led to a sharp decrease in the PBT peak(s) and a strong appearance of the peaks characteristic of $BaTiO_3$. This can be attributed to the shielding effect for high intensity diffraction patterns of $BaTiO_3$ [26]. Independent of filler volume fraction the XRD peak intensities of the composites showed almost no change, which is attributed to little or no change in $BaTiO_3$ crystalline stability. X-ray diffraction plots for the LLDPEBT composites are shown in Figure 4 (d) and apart from PBTBT structures, it is observed that the characteristic LLDPE pattern located at 25° is present, particularly in LLDPEBT10 and LLDPEBT20 samples. Thus, it can be concluded that the crystal phase of LLDPE is more prominent for these samples as compared to other LLDPEBT systems while the addition of more filler resulted in the disappearance of LLDPE peaks.

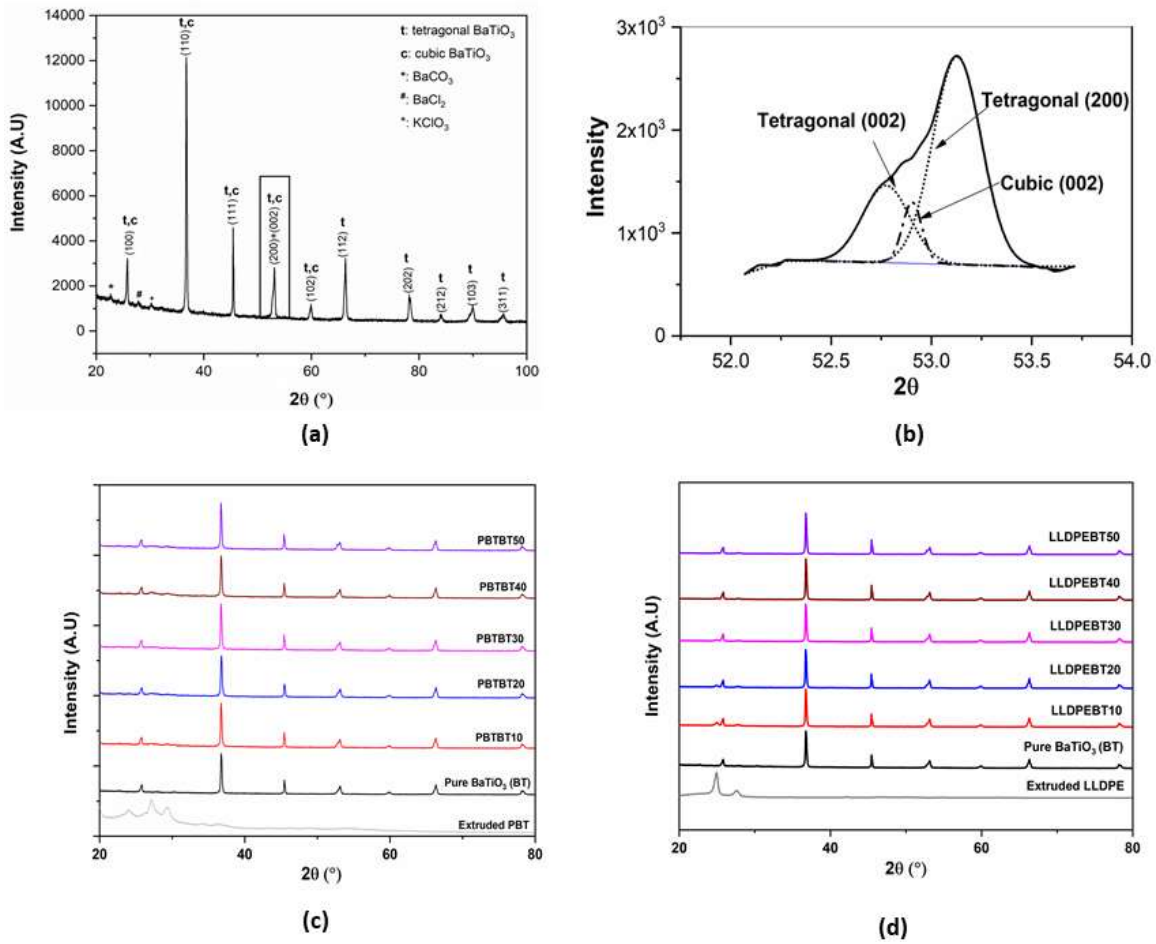


**Figure 4.** XRD diffraction patterns of a) $BaTiO_3$, (b) (200) and (002) tetragonal and cubic plane patterns of $BaTiO_3$ at 2θ~53°, (c) PBTBT and (d) LLDPEBT composites.

3.3. FTIR Analysis

Figure 5 (a) shows the FTIR absorbance spectra for pure PBT, as-received $BaTiO_3$ and the PBTBT samples to reveal whether a specific chemical and/or physical interaction occurs between the constituents of the composites. Characteristic IR bands for neat PBT observed at 2958 $cm^{-1}$ and 1708 $cm^{-1}$ correspond to the $CH_2$ stretching and C=O stretch, respectively. Additionally, the peak at 1460 $cm^{-1}$ is assigned to C-H bending in $CH_2$ groups while the peaks

at 1409 $cm^{-1}$ and 1014 $cm^{-1}$ are attributed to bending of aromatic rings in PBT chains. The bands that appear at 1242 $cm^{-1}$, 1097 $cm^{-1}$, 873 $cm^{-1}$ and 725 $cm^{-1}$ are ascribed to CO-O stretching in esters, O-$CH_2$, aromatic out of plane C-H bending and aromatic C-H bending ($CH_2$ rocking), respectively [27]. The characteristic IR peaks of PBT are all present in the spectra recorded for the composites. The unique absorption peak, associated with $BaTiO_3$ at 1436 $cm^{-1}$ is attributed to carbonate ion impurities and observed in the same figure [28]. In the case of PBTBT composites, this peak is embedded in the IR spectra thereby suggesting no apparent interaction between polymer and ceramic components.

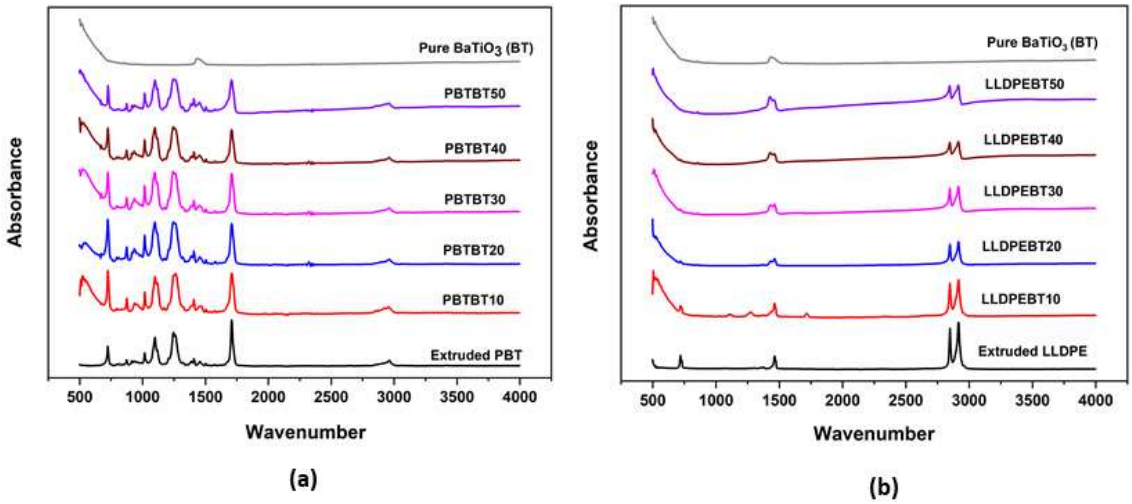


**Figure 5.** FTIR spectrum of (a) PBTBT and (b) LDPEBT composites.

The FTIR spectra of the LLDPEBT composites are shown in Figure 5 (b). Although the characteristic LLDPE IR bands are observed for all composite samples it is noteworthy that the LLDPE peak at 1467 $cm^{-1}$, which corresponds to $CH_2$ bending, and the $BaTiO_3$ peak at (1436 $cm^{-1}$) overlap and a doublet of peaks is seen. The peak detected at 730 $cm^{-1}$ for LLDPE, attributed to $CH_2$ rocking is less intense for the composite with 10 vol.% $BaTiO_3$

(LLDPEBT10), but has disappeared in the spectra of the composites with higher $BaTiO_3$ loading. The major LLDPE peaks at 2845 $cm^{-1}$ and 2910 $cm^{-1}$ correspond to C-H stretching [29]. As expected, as the $BaTiO_3$ loading is increased the increase in particle volume fraction greatly affects the IR peak intensities, which can be attributed to the functional group decrease associated with molecular bonds [30].

3.4. Thermal Analysis (DSC and TGA)

The effect of $BaTiO_3$ content on polymer crystalline content and the melting and crystallization behaviour of the composites were studied using DSC. Figure 6 (a) and (b) shows the thermograms for the first cooling and second heating steps (a first heating step was used to eliminate the thermal history of the sample of interest) for unfilled PBT as well as $BaTiO_3$-filled PBT. From these graphs the melting temperature ($T_m$), crystallization temperature ($T_c$), crystallization enthalpy ($H_c$), melting enthalpy ($H_m$) and degree of crystallinity ($X_c\%$) were determined and are reported in Table 2. The percentage crystallinity of the composites was determined using equation 1:

$$X_c = \frac{\Delta H_m}{\Delta H_m^0 (1 - X_f)} \times 100 \qquad (\mathbf{1})$$

where $X_f$, $\Delta H_m$ and $\Delta H_m^0$ represent the weight fraction of filler, melting enthalpy (heat of fusion) of the sample of interest and for a theoretically 100% crystalline polymer, respectively [23]. For the latter $\Delta H_m^0$ for PBT and LLDPE were taken as 140J/g and 290 J/g, respectively [23,31]. From the cooling thermograms (Figure 6-a), extruded unfilled PBT had

$T_c$ = 192°C while the composites had $T_c$ in the range 195-198°C. This increase (3-6°C compared to extruded unfilled PBT) indicates that barium titanate acted as a nucleating agent for PBT and accelerated the crystallization kinetics of PBT. In order to investigate the $T_m$ characteristics of the PBTBT composites, the DSC heating curves were examined (Figure 6-b). These thermograms for the as-extruded PBT and PBTBT composites displays double/multiple peak formation, which is attributed to melting-recrystallization-remelting processes. The thermograms for the composites showed extra minor peaks at slightly lower temperatures below the main peaks, independent of filler concentration. The appearance of this combination of endothermic peaks is related to the variation in PBT crystal structure, size and packing efficiency, as well as the variation in crystallite thicknesses [23,32].

From Figure 6 (c), the $T_c$ of the LLDPE based composites was 4 to 5.5°C greater than that of unfilled LLDPE while the $T_m$ values were similar. As was the case for the PBTBT composites, inclusion of $BaTiO_3$ in LLDPE results in an increase in $T_c$ because of the promotion of heterogeneous nucleation of LLDPE [33,34]

Clearly, as the volume fraction of $BaTiO_3$ increases the crystalline content of all composites decreased significantly, independent of polymer type (Table 2). It should be noted here that $X_c\%$ values were calculated by considering the mass fraction determined from TGA data converted to volume fraction. According to literature, throughout the polymer recrystallization process, the reinforcement/filler phase can either promote nucleation and lead to increased crystallinity or behave as a physical obstruction, hinder crystallization and result in lower crystallinity [35]. In our work, the restricted mobility of polymer chains in the presence of the $BaTiO_3$ hinders the rearrangement of macromolecular segments in the

formation of crystal phases [32,36]. Due to the relatively high ceramic phase content (>10vol.%), the loss of crystalline phase was between 35%-50% with the addition of $BaTiO_3$.

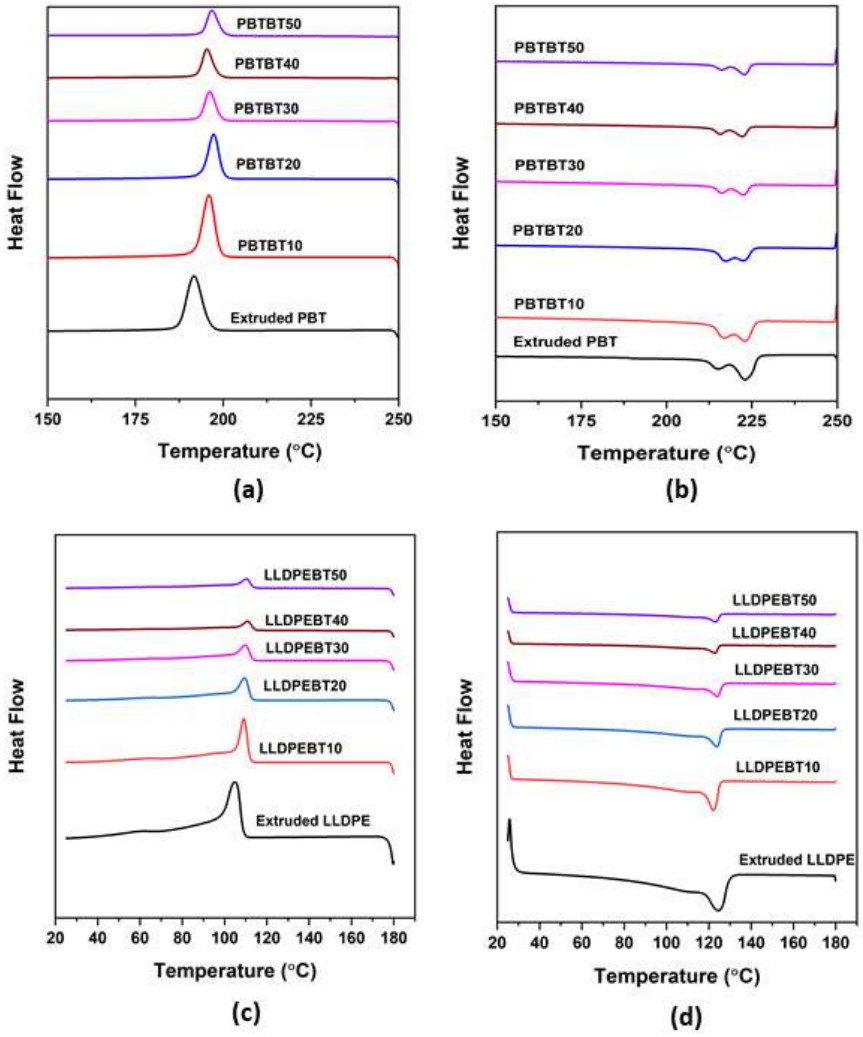


**Figure 6.** DSC thermograms showing (a) crystallization exotherms and (b) melting endotherms of extruded PBT and PBTBT composites and, (c) crystallization exotherms and (d) melting endotherms of extruded LLDPE and LLDPEBT composites.

**Table 2.** Thermal properties of composites of LLDPE or PBT and $BaTiO_3$ determined from DSC measurements.

| Material Type | $T_m$ (℃) | $\Delta H_m$ (J/g) | $T_c$ (℃) | $\Delta H_c$ (J/g) | $X_c$% |
|---|---|---|---|---|---|
| PBT | 222.7 | 61.9 | 192.1 | 35.9 | 44.2 |
| PBTBT10 | 222.4 | 28.1 | 196.7 | 32.5 | 29.3 |
| PBTBT20 | 216.9 | 19.9 | 197.9 | 24.3 | 23.7 |
| PBTBT30 | 222.1 | 13.1 | 196.6 | 18.4 | 22.1 |
| PBTBT40 | 221.9 | 11.1 | 195.8 | 15.4 | 23.8 |
| PBTBT50 | 222.4 | 9.8 | 197.2 | 21.9 | 25.2 |
| LLDPE | 124.2 | 96 | 105.3 | 100.7 | 33.1 |
| LLDPEBT10 | 122.1 | 53.2 | 109.3 | 60.1 | 27.6 |
| LLDPEBT20 | 123.6 | 34.8 | 109.5 | 41.2 | 26.5 |
| LLDPEBT30 | 123.8 | 25.1 | 110 | 29.8 | 24 |
| LLDPEBT40 | 122.9 | 16.8 | 110.9 | 23 | 21.2 |
| LLDPEBT50 | 123.2 | 14 | 110.4 | 19.6 | 22.9 |

The thermal stability as well as relative ceramic content of the composites were also studied using thermgravimetric analysis (TGA) (Figure 7). The as-extruded PBT, Figure 7 (a), exhibits a main degradation step up to 430°C followed by a further mass loss in the form of a shoulder process. The range of thermal decomposition for neat PBT is between 352°C and 600°C. Based on the same Figure only 0.5wt.% PBT was present after 600°C while

$BaTiO_3$ did not lose any mass between 25°C and 800°C due to its high melting temperature (1625°C). Introduction of $BaTiO_3$ led to the contraction of the decomposition ranges for each composite system to different levels, as expected. The parameters related with TG data are shown in Table 2 where $T_{10\%}$, $T_{peak}$ and $T_{decomp.range}$ represent the temperature at 10% weight loss, maximum mass change temperature, and temperature range for thermal degredation, respectively. The PBTBT samples exhibited one decomposition process, see Figure 7. From Table 3, the onset temperature of thermal degradation in the composites (i.e. 370-382°C) are close to each other and higher, compared to extruded neat PBT. Based on the derivative TGA data shown in Figure 7(c), the maximum change in the rate of mass loss ($T_{peak}$) for the PBTBT samples did not change with increasing ceramic content. Furthermore, the $T_{10\%}$ values were also reported for the composites and the presence of more $BaTiO_3$ shifted these temperatures to higher values (~25-31°C increments), which can be attributed to the improved interaction between PBT and $BaTiO_3$ [37]. The TGA graph of extruded LLDPE (Figure 7-b) showed a non-homogeneous degradation process where the onset and end decomposition temperatures were determined as 370°C and 561°C, respectively. The incorporation of filler caused the narrowing of the decomposition domains for LLDPEBT composites depending on the $BaTiO_3$ content. Additionally, the decomposition range ($T_{decomp.range}$) of LLDPEBT samples increased with the addition of ceramic particles up to 20 vol.% (theoretical). As the volume fraction of $BaTiO_3$ was increased further, the linkage between the filler and polymer matrix decreased due to the agglomeration of particles, which led to the reduced decomposition temperature [38]. The $T_{10\%}$ parameter for the same composites, which has been used as an indicator of thermal stability, achieved higher values

compared to the extruded LLDPE matrix. The temperatures of maximum loss for the LLDPEBT samples were obtained by considering derivative TG data in Figure 7 (d), and depicted in Table 3. The peak temperature was determined as the highest maximum of the DTG graph [39]. Among all LLDPEBT composites, no remarkable improvement was observed in terms of $T_{peak}$ with the incorporati on of ceramic powder. According to Table 3, the LLDPEBT50 structure showed significantly lower $T_{peak}$ value (467°C), which can be attributed to the heat source zones to speed up the decomposition of matrix during the thermal degredation [40].

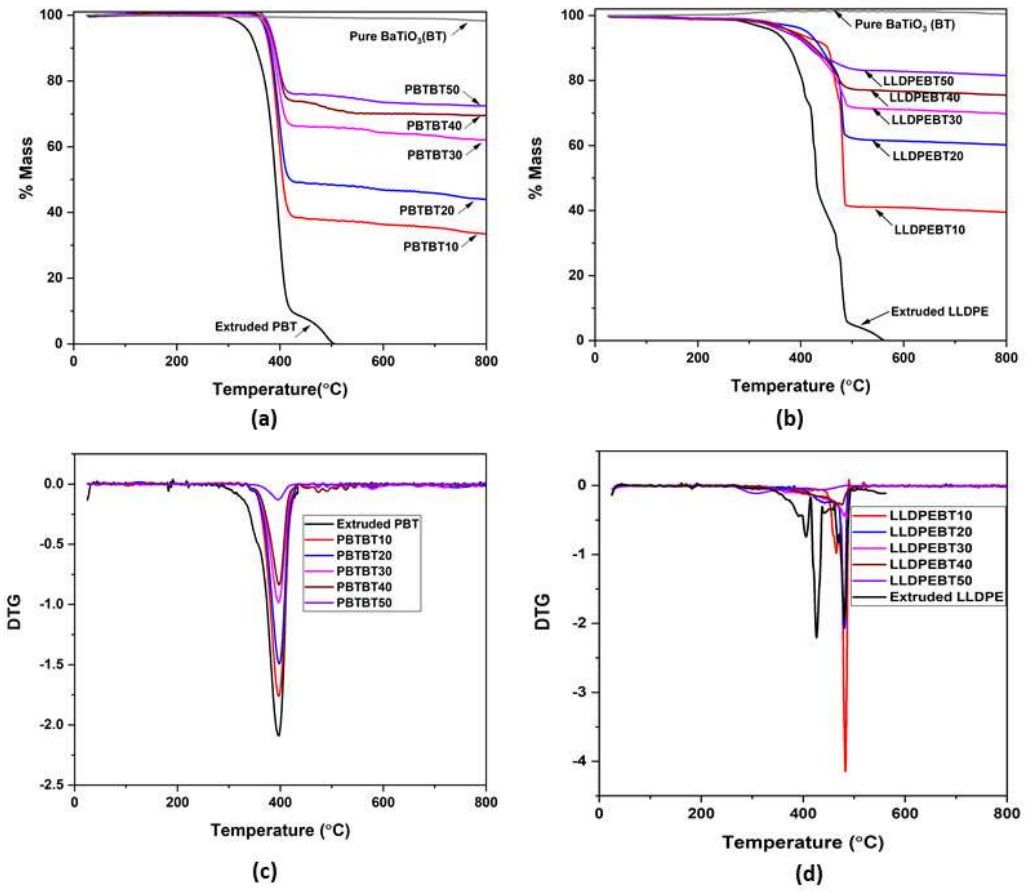

**Figure 7.** TGA weight loss curves for (a) extruded PBT and PBTBT composites, (b) extruded LLDPE and LLDPEBT composites, (c) DTG curve of PBTBT composites and (d) DTG curve of LLDPEBT composites.

**Table 3.** TGA parameters for PBT, LLDPE, $BaTiO_3$ and composites of PBT or LLDPE and $BaTiO_3$.

| **Material Type** | $T_{10\%}$ **(°C)** | $T_{peak}$ **(°C)** | $T_{decomp.range}$ **(°C)** | **Residual volume @ 800°C (vol.%)** | **Volume calculated from Archimedes' Density (vol.%)** | **Relative density (%)** |
|---|---|---|---|---|---|---|
| PBT | 354 | 394 | 352-600 | 0.85 | - | - |
| PBTBT10 | 379 | 401 | 370-800 | 9.5 | 9.2 | 85 |
| PBTBT20 | 382 | 399 | 373-800 | 13.2 | 12.9 | 81.2 |
| PBTBT30 | 385 | 400 | 375-795 | 23.7 | 18.8 | 78.7 |
| PBTBT40 | 389 | 398 | 379-790 | 31.3 | 29 | 71.9 |
| PBTBT50 | 391 | 398 | 382-785 | 39.6 | 43.1 | 88.3 |
| LLDPE | 377 | 481 | 370-561 | 0.02 | - | - |
| LLDPEBT10 | 452 | 482 | 444-794 | 7.7 | 9.8 | 98 |
| LLDPEBT20 | 439 | 481 | 407-793 | 16.6 | 19.7 | 98 |
| LLDPEBT30 | 421 | 486 | 367-795 | 22.7 | 27.2 | 93 |
| LLDPEBT40 | 425 | 478 | 370-790 | 30.5 | 36.8 | 93.5 |
| LLDPEBT50 | 386 | 467 | 337-790 | 38.2 | 48.2 | 97 |

The weight percentages of composites at 800°C were converted into volume fractions by considering the TGA residual mass data and given in Table 3. Also the relative densities of samples were added to the same table. This parameter was calculated from the ratio of the bulk density ($\rho_{bulk}$) and Archimedes' density ($\rho_{Archimedes}$) that were determined from the Archimedes' method and volumetric mixing law, respectively. As can be seen in the same table, the theoretical and experimental volumetric ratios of the composites exhibited notable variations, which can be ascribed to the very small TGA specimen mass/size. Archimedes' density measurements that use larger specimens and contain more composite mass were carried out to confirm/compare the TGA results. Based on the Archimedes' density results, the actual volume fraction of PBTBT composites were approximately 7-10% lower than the theoretical values, which is attributed to the lack of packing and/or integration between ceramic filler and polymer medium during extrusion. However LLDPEBT compositions were in a good agreement with the $BaTiO_3$ quantities that were weighed during the specimen preparation. Relative density measurements confirmed the aforementioned results and it was seen that LLDPEBT samples showed higher values for this parameter in comparison with PBTBT counterparts.

### 3.6. Dielectric Analysis

The effect of the $BaTiO_3$ concentration on the dielectric properties of the composites was investigated in the frequency range 2.45-5 GHz, a range most commonly used for wireless applications. Transmission line and free space method with coaxial probe was utilized during analysis with two port vector network analyzer-VNA (Keysight™ E5063A). The required

sample thickness for each composition was calculated using the VNA analysis software which determines the theoretical dielectric permitivitty (real part of permitivitty) for the composites from the extracted S-parameters measured by the VNA. The Lichtenecker equation [24,41] (equation 2) was utilized to estimate this parameter. Here $\varepsilon'_m$, $\varepsilon'_f$ and $\varepsilon'_{eff}$ represent the permittivity of the polymer matrix, filler and composite, respectively while "$f$" is the filler volume fraction which was determined from the Archimedes' density measurements described above. In this study the $\varepsilon'_m$ values of PBT and LLDPE polymers were determined as 3.7 [42] and 2.5 [43], respectively and $\varepsilon'_f$ for $BaTiO_3$ was estimated to be 500 [24,44].

$$ln\,\varepsilon'_{eff} = f\,ln\,\varepsilon'_f + (1-f)\,ln\varepsilon'_m \qquad \textbf{(2)}$$

Figure 8 (a) and (b) show the frequency dependent dielectric responses of the PBTBT and LLDPEBT composites as a function of $BaTiO_3$ loading. No substantial dielectric relaxation was observed through the analysis and the samples showed stable performance through this frequency range, which is also favourable for various electronic applications. Although the presence of $BaTiO_3$ enhances the permittivity of the composites due to its higher $\varepsilon'$ value, polymer type (polar PBT or non-polar LLDPE) and particularly powder content (vol.%) dominates the overall dielectric response. Therefore, the PBTBT and LLDPEBT composites exhibited different $\varepsilon'$ values as seen in Figure 8(a) and 8(b), respectively. As expected, the $\varepsilon'_{eff}$ of the composites increased as the $BaTiO_3$ content increased. In this study at 2.45 GHz, the permittivity of pure PBT and LLDPE were measured as 3.3 and 2.3, respectively. The

PBTBT50 composite exhibited 6.5 times higher permitivitty (i.e. 21.2 for ~43 vol.% $BaTiO_3$) as compared to neat PBT while the LLDPEBT50 specimen showed about 10 times greater permittivity (i.e 25 for ~48 vol.% $BaTiO_3$) compared to unfilled LLDPE. The increase in permitivitty for the composites with higher $BaTiO_3$ content can be attributed to the polarisable groups within the $BaTiO_3$ powder. As the occupation of these groups per unit volume in the composites increases, permittivity is significantly enhanced [25,45]. The magnitude of loss tangent (dissipation factor or $tan\delta$) also provides important information about the dielectric characteristics of the composite materials. The dissipation factor behaves in a more complicated manner as seen in Figure 8 (b). The $tan\delta$ values of PBTBT specimens generally indicated relatively less dispersion compared to the LLDPEBT counterparts between 2.45-5 GHz. For higher $BaTiO_3$ concentration, particularly above 20% actual volume loading, the loss tangent for the PBTBT samples exhibited relatively higher magnitudes. For instance at 2.45 GHz, this variable was only 0.006 for unfilled PBT but 0.015 for the PBTBT50 composite at the same frequency. In comparison, neat LLDPE had a $tan\delta$ = 0.0003 at 2.45 GHz, and the dissipation factor of corresponding composites generally increased with increasing $BaTiO_3$ content, e.g. $tan\delta$= 0.009 at 2.45 GHz for the LLDPEBT50 composite. Although polar polymers provide a positive contribution to dielectric properties, no real improvement was obtained for the PBT-based composites in this study. Rather, non-polar LLDPE based composites achieved better performance due to more filler content, behaviour possibly related to the higher packing capability of $BaTiO_3$ in LLDPE during processing [45].

Table 4 compares the permittivity and loss tangent values of this study with those of $BaTiO_3$ loaded polymer composites in the literature by considering volumetric concentrations and particle size parameters. As reported in the literature, besides these two parameters, crystal structure of filler, processing conditions, matrix characteristics, particle content and frequency range significantly affect the dielectric responses of composites. At relatively lower frequency band (generally up to maximum 1 MHz) interfacial polarization (space charge polarization) mechanism contributes to the increase of dielectric permittivity, particularly for the highly loaded composites. However, as the frequency increases, polarization becomes more difficult due to time constraints, which results in a decrease in permittivity [46]. Similar observations were made in the studies listed in Table 4. It seems that the composites generally exhibited higher permittivity values in the low frequency domain [24,47-48]. The inrease in frequency resulted in a reduction of dielectric permittivities independent of $BaTiO_3$ concentration and particle size. However, the loss tangent values for the composites did not show a frequency dependent behavior and in some cases that parameter decreased as the frequency increased [48].

Based on dielectric measurements conducted in this work, it was observed that both PBTBT and LLDPEBT composites exhibited remarkable values throughout the wireless (Wi-Fi) requency range (2.45-5 GHz). Therefore, our samples would display higher permittivity values at lower frequencies compared to the polymer/$BaTiO_3$ composites given in Table 4.

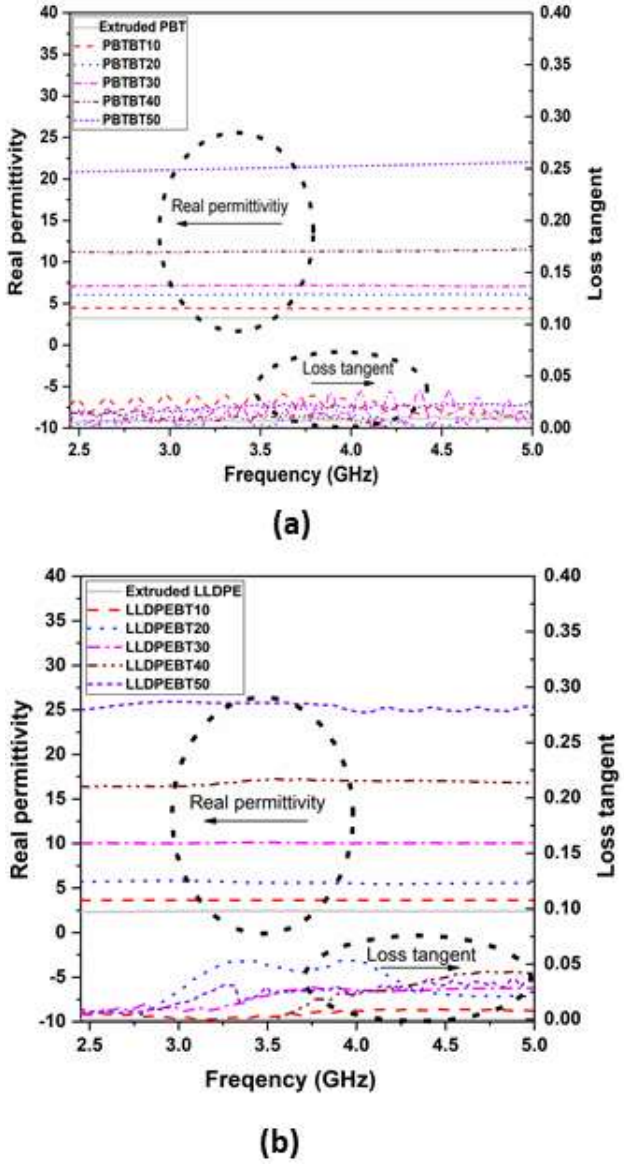


**Figure 8.** Variation in permittivity and loss tangent for (a) PBTBT and (b) LLDPEBT composites.

**Table 4.** Real permittivity value comparsions of $BaTiO_3$/polymer based composites

| Polymer Matrix | $BaTiO_3$ loading | $BaTiO_3$ size(nm) | Real Permittivity (ε') | Loss tangent (*tanδ*) | Reference |
|---|---|---|---|---|---|
| (PFA) | ~29 vol.% | 300 | 14 @10 kHz | ~0.08 @10 kHz | 24 |
| | 20 vol.% | | 6 @ (12-18 GHz) | ~0.03-0.035 @ (12-18 GHz) | |
| [P(VDF-HFP)] | 40 vol.% | 60 | 32 @1 MHz | ~0.16@1 MHz | 35 |
| PA-11 | 40 vol.% | 500 | 17 @ 1 MHz | N.A | 47 |
| | | | 16 @ 10 MHz | N.A | |
| HDPE | 50 vol.% | 1600 | 30 @ 40 Hz | 0.103 @ 40 Hz | 48 |
| | | | 19 @ 40 MHz | 0.012 @40 MHz | |
| PVDF | 60 wt.% | 2320 | 15 @ 1 MHz | ~0.45@ 1 MHz | 49 |
| PVDF | 70 wt.% | 100 ≤ | 9 @ (2-5 GHz) | 0.01@ (2-5 GHz) | 50 |
| PBT | 43 vol.% | 400 | 21 @(2.45-5 GHz) | 0.015-0.023 @ (2.45-5 GHz) | This work |
| LLDPE | 48 vol.% | | 25 @(2.45-5 GHz) | 0.009-0.03 @ (2.45-5 GHz) | |

Figure 9 (a) and (b) compare the experimental data and theoretical predictions for the permittivity of the composites at 2.45 GHz. From Figure 9 (a), the experimental $\varepsilon'_{eff}$ of the composites at lower $BaTiO_3$ content (i.e. up to 20 vol% - actual value for PBTBT30) are in

good agreement, as expected. The same parameter deviated for the PBTBT40 and PBTBT50 composites, which may be attributed to effects such as agglomeration of the $BaTiO_3$ particles, porosity, interface morphology between composite components, homogeneous dispersionand crystal morphology of the $BaTiO_3$ particles [47-50]. With regard Figure 9(b), the same analytical approach was carried out for the LLDPEBT composites where better agreement between experimental and theoretical values was obtained relative to the PBTBT counterparts. However, as the $BaTiO_3$ content increased up to ~50vol.%, the dielectric permitivitty of LLDPEBT50 sample showed some divergence. Moreover, the presence of 30% cubic phase in $BaTiO_3$ may contribute to reduction in the maximum permittivity.

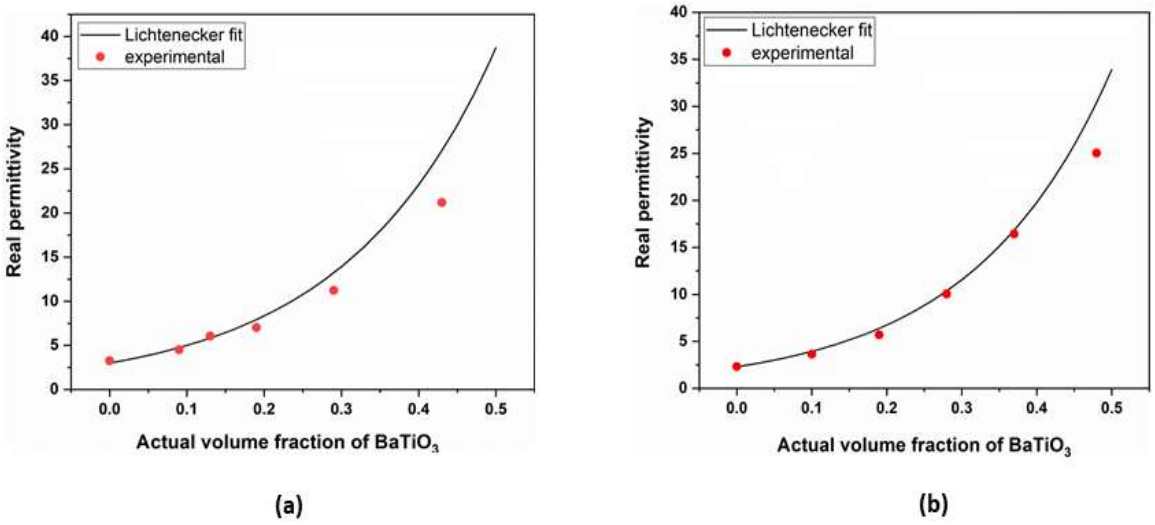


**Figure 9.** Comparison of experimental and theoretical dielectric permitivitty of (a) PBTBT composites and (b) LLDPEBT composites at 2.45 GHz.

## 4. Conclusions

Perovskite $BaTiO_3$ powder consisting of 30% cubic and 70% tetragonal phases was blended with polar PBT and non-polar LLDPE at volume fractions up to 0.5 using melt extrusion. Although no prominent chemical modification was observed with the incorporation of ceramic filler, the composites generally showed fine particle dispersion and distribution in the polymer matrices. Based on thermal analysis and Archimedes' density measurements, the LLDPEBT composites showed higher actual volume fractions compared to the PBTBT counterparts. Although $BaTiO_3$ particles acted as a nucleation agent for the polymers and increased the crystallization temperature slightly, the crystalline content of the composites decreased as the filler content increased. The permittivity of the composites was experimentally measured between 2.45-5 GHz and the Lichtenecker model used to estimate the theoretical dielectric permitivitty ($\varepsilon'_{eff}$) of the composites. The $\varepsilon'_{eff}$ values of the composites significantly increased as the ceramic concentration was increased, due to enhanced polarization and connectivity between $BaTiO_3$ particles. At 2.45 GHz, the ~48 vol% ceramic loaded LLDPEBT50 composite had a real permittivity of 25 while that for the PBTBT50 composite with 43 vol% filler was 21.2. From the experimental results, the predicted $\varepsilon'_{eff}$ values showed relatively higher deviations as the particle concentration increased. Similar to real permitivitty, the loss tangent data for the composites generally increased with the introduction of increasing ceramic loadings. Therefore, both PBTBT and LLDPEBT composites are potential candidates for capacitor applications, particularly in the microwave frequency range.

**Acknowledgement**

The authors acknowledge the Scientific and Technological Research Council of Turkey (TÜBİTAK) International Post Doctoral Research Fellowship Programme (BİDEB-2219) who funded this work. Bahar Basturk thanks the IINM, WMG, University of Warwick for hosting her research visit.

**References**

1. L. Xie, X. Huang, Y. Huang, K. Yang, P. Jiang, ACS Appl. Mater. Interfaces. **2013**, 5, 1747.
2. P. Barber, S. Balasubramanian, Y. Anguchamy, S. Gong, A. Wibowo, H. Gao, H.J. Ploehn, H. Zur Loye, Materials. **2009**, 2, 1697.
3. P. Thomas, K.T. Varughese, K. Dwarakanath, K.B.R. Varma, Comp. Sci. Tech. **2010**, 70, 539.
4. P. Thomas, S. Satapathy, K. Dwarakanath, K. B. R. Varma, Express. Polym. Lett. **2010**, 4, 632.
5. P.S. Anjana, V. Deepu, S. Uma, P. Mohanan, J. Philip and M.T. Sebastian, J. Polym. Sci. B Polym. Phys. **2010**, 48, 998.
6. J. Li, J. Claude, L. E. Norena-Franco, S. Seok, Q. Wang, Chem. Mater. **2008**, 20, 6304.
7. G. Gallone, F. Carpi , D. De Rossi, G. Levita, A. Marchetti, Mater. Sci. Eng. C. **2007**, 27, 110.
8. S. Ogitani, S. A. Bidstrup-Allen, P. A. Kohl, IEEE Trans. Adv. Packag. **2000**, 23, 313.
9. Y. Bai, Z.-Y. Cheng, V. Bharti, H. S. Xu, Q. M. Zhang, App. Phys. Lett. **2000**, 76, 3804.

10. L. Bingcheng, W.X. Wang, Y. Wang and L.Li, J. Mater. Chem. A. **2014**, 2, 510.
11. A. Pelaiz-Barranco, Scr. Mater. **2006**, 54, 47.
12. D. Yang, L. Zhang, H. Liu, Y. Dong, Y. Yu, M. Tian, J. Appl. Polym. Sci. **2012**, 125, 2196.
13. T. Anil Babu, K.V. RamesH, R.V. Reddy, D.L. Sastry, Mat. Sci. Eng. B. **2018**, 228, 175.
14. A. Peláiz-Barranco, P. Marin-Franch, J. Appl. Phys. **2005**, 97, 034104.
15. Y. Kobayashi, T. Tanase, T. Tabata, T. Miwa, M. Konno, J. Eur. Ceram. Soc. **2008**, 28, 117.
16. Y. Hao, X. Wang X, K. Bi, J. Zhang, Y. Huang, L. Wu, P. Zhao P, X. Kun, L. Ming, L.Longtu, Nano Energy. **2017**, 31, 49.
17. S.K. Gupta, K.N. Pandey, V. Verma, S. Mathur, V. Kumar, Appl. Polym. Compos. **2013**, 1, 47.
18. S. Xie, B.K. Zhu, X.Z. Wei, Z.K. Xu, Y.Y. Xu, Comp. Part A. **2005**, 36, 1152.
19. J. Topham, O. Boorman, I.L. Hoiser, M. Praeger, R. Torah, A.S. Vaughan, T. Andrritch, S.G. Swingler, IEEE Conf. on Elec. Insulation and Dielectric Phen. (CEIDP), Des Moines, IA, 711-714, **2014.**
20. W. Yang, S. Yu, S. Luo, R. Sun, W.H. Liao, C.P. Wong, J. Alloy. Compd. **2015**, 620, 315.
21. S. Koulouridis, G. Kiziltas, Y. Zhou, D. J. Hansford, J. L. Volakis, IEEE Trans. Microw. Theory. Tech. **2006**, 54, 4202.
22. C. K. Chiang, R. Popielarz, Ferroelectrics .**2002**, 275, 1.

23. J. Bian, H.L.Lin, F.X. He, L. Wang, X.W. Wei, I.T. Chang, E. Sancaktar, Eur. Polym. J. **2013**, 49, 1406.

24. Grant, PS, CRM Grovenor, Q Lei, CEJ Dancer, Comp. Sci. Tech. **2016**, 129, 198.

25. Z. Wang, J.K. Nelson, J. Miao, R.J. Lindhardt, L.S.Schadler, IEEE Trans. Dielectr. Electr. Insul. **2012**, 19, 960.

26. J. Fu, Y. Hou, M. Zheng, Q. Wei, M. Zhu, H.Yan, ACS Appl. Mater. Interfaces .**2015**, 7, 24480.

27. Katti D.R, Katti K.S, Raviprasad M, Gu C, J. Nanomater, **2012**, 2012(28).

28. Pant H.C, Patra M.K, Verma A, Vadera S.R, Kumar N, Acta Mater. **2006**, 54, 3163.

29. J. Melissa R, H. F David, O. Sara V, R. C Viviana, B. Kathryn L, B. George H, J. T Todd, W. Thierry M, B. Kayla C, R.Sarah-Jeanne, H. K David, J. Brenda A, L. JenniferM, Mar. Pollut. Bull. **2018**, 127, 704.

30. Marek W. Urban, Vibrational Spectroscopy of Molecules and Macromolecules on Surfaces, Wiley **1993**.

31. S. Paszkiewicz, A. Szymczyk, D. Pawlikowska, J. Subocz, M. Zenker, R. Masztak, Nanomaterials (Basel), **2018**, 8, 264.

32. O. Saligheh, M. Forouharshad, R. Arasteh, R. Eslami-Farsani, R. Khajavi, B. Yadollah Roudbari, J. Polym. Res. **2013**, 20.

33. Y.C. Li Y, S.C. Tjong, R.K.Y. Li, Express Polym. Lett. **2011**, 5, 526.

34. J. Li, J. Claude, L.E. Norena-Franco, S. Seok, Q. Wang, Chem. Mater. **2008**, 20, 6304.

35. X. Lu, X. Zou, J. Shen, L. Jin, F. Yan, G. Zhao, L. Zhang, Z.Y. Cheng, Ceram. Int. **2019**, 45, 17758.

36. G.S. Deshmukh, D.R. Peshwe, S.U. Pathak, J. Ekhe, J. Polym. Res. **2011**, 18, 1081.

37. T. K. Bindu Sharmila, J. V. Antony, M. P. Jayakrishnan, P. M. Sabura Beegum, E. T. Thachil, Mater. Des. **2016**, 90, 66.

38. R. Wang, C. Xie, L. Zeng, H. Xu, RSC Adv. **2019**, 9, 790.

39. A.A. Al-Ghamdi, F. El-Tantawy, Compos.Part A. Appl. Sci. Manuf. **2010**, 41, 1693.

40. J. Xie, H. Wang, Z. Wang, Q. Zhao, Y. Yang, G.I.N. Waterhouse, L. Hao, Z. Xiao, J. Xu, Sci. Rep. **2018,** 52, 1.

41. J. Chameswary, M.T. Sebastian, J. Mater.Sci: Mater. Electron. **2015**, 26, 4629.

42. L. Cadillon Costa, S. Devesa, P. André, e-Polymers Short Communications. **2005**, No: 004.

43. A. Dabbak, S.Z. Illias, H.A. Ang, B.C. Abdul, N.A. Latiff, M.Z.H. Makmud, Energies. **2018**, 11, 1448.

44. C. Offenzeller, M.A. Hintermüller, W. Hilber, B. Jakoby, Microelectron. Eng. **2020**, https://doi.org/10.1016/j.mee.2020.111220.

45. R. Popielarz, C. K. Chiang, R. Nozaki, J. Obrzut, Macromolecules. **2001**, 34 (17), 5910.

46. W. Yang, Y. Shuhui, R. Sun, W.H. Liao, C.P. Wong, J. Alloy. Compd. **2015**, 620, 315.

47. F. Qi, N. Chen, Q. Wang, Mater. Des. **2017**, 131, 135.

48. J. Su, J. Zhang, J. Polym. Sci. B. Polym. Phys. **2018**, 56, 1101.

49. E. Ruggiero, M.M. Reboredo, M.S. Castro, J. Compos. Mater. **2017**, 52, 1399.

50. L. Yu, Y. Zhu, Y. Fu, RSC Adv. **2017**, 7, 36473.